Journal of Materials Chemistry B

Accepted Manuscript

ROYAL SOCIETY OF CHEMISTRY

www.rsc.org/materialsB

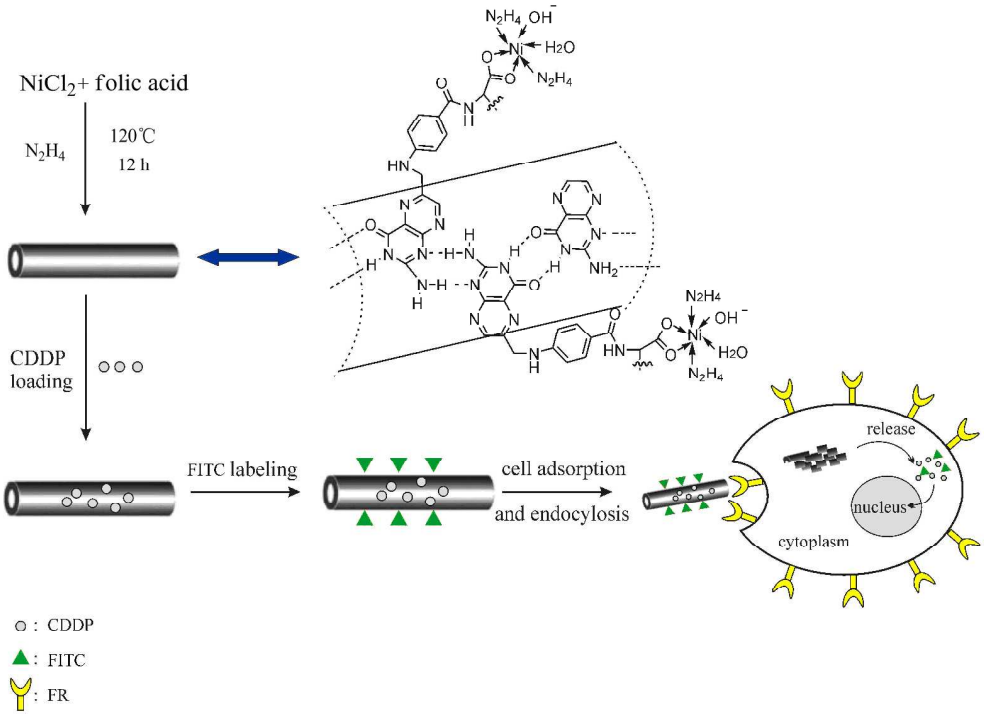

The biomolecule-based Ni folate-hydrazine coordination complex nanotubes (BMB-CCNTs) have been constructed effectively by using solvothermal method. The BMB-CCNTs are stable enough at normal physical pH 7.4 until entering tumor cell, but break up to release drug in tumor cell. The antitumor ability of BMB-CCNTs own is similar to cisplatin (CDDP) in vitro, while cytotoxicity for normal cell is less than CDDP. Furthermore, BMB-CCNTs exhibit excellent performance as drug carrier and target agent for delivering drug into tumor cells.

Journal of Materials Chemistry B

Cite this: DOI: 10.1039/c0xx00000x

www.rsc.org/xxxxxx

ARTICLE TYPE

Synthesis, characterization and anticancer activity in vitro of the biomolecule-based coordination complex nanotubes

Yue Wang, [a,b] Chi Zhang, [a] Hongmei Li, [b] Guoxing Zhu, [a] Song-Song Bao, [a] Shiqiang Wei, [a] Li-Min Zheng, [a] Min Ren, [a] and Zheng Xu*[a]

Received (in XXX, XXX) Xth XXXXXXXXX 20XX, Accepted Xth XXXXXXXXX 20XX
DOI: 10.1039/b000000x

The biomolecule-based coordination complex nano-assemblies are the kind of new growing functional materials, which could possess functionalities that are not readily attainable with other materials and is a full of promise research area to exploit in coordination chemistry and material science. Using bio-active folic acid molecule as a linker, Ni folate-hydrazine coordination complex nanotubes (CCNTs) had been constructed effectively by using solvothermal method. It is not only the first example of the CCNTs formed by using non-pyridyl-based molecule as a linker, but also the first report on the biomolecule-based CCNTs (BMB-CCNTs) with anticancer activity. It is no need to do any post treatment to get targeting deliverable and biocompatible performance. The BMB-CCNTs are stable enough at normal physical pH 7.4 until entering tumor cell, but break up to release drug in tumor cell. Furthermore, it overcomes the main limitations of antibody-drug and folate-drug conjugates and is a potential smart multi-functional nanomedicine system. The results of cytotoxicity assay in vitro reveal that the antitumor ability of BMB-CCNTs own is similar to cisplatin (CDDP), while cytotoxicity for normal cell is less than the latter. Furthermore, BMB-CCNTs exhibit excellent performance as drug carrier and target agent for delivering drug into tumor cells. Bio-TEM and confocal laser scanning microscope images trace the uptake process of CDDP-CCNTs by tumor cell. CDDP-CCNTs exhibit dual anti-cancer effect.

Introduction

Coordination complex nano-assemblies are the kind of new growing functional materials, which exhibit a high level of composition selectivity, structural tailorability and function tunableness. It is predicted possessing functionalities which is not ready attainable with other materials. Depending on metal types, its oxidation states and coordination number, various geometries of coordination complexes can be obtained. At the same time, the ligand nature can also lead to different linking sites with tuned binding strength and directionality. The structures of formed complex dictate the formation, organization and function of discretely defined nano-assemblies. So, use of geometrically demanding metal-ligand framework is a promising strategy to fabricate structurally defined functional nanomaterials.

Although some works have been reported, [1-4] the most present study of coordination chemistry still focuses on the bulk crystalline solids such as nano-channel porous solids, even so, it is still a challenge to design metal-organic frameworks (MOFs) with a designed structure and function based on a given set of metal complexes and ligands, whereas the discretely defined nano-assemblies with shape control are largely unexplored. Our group and others [5-10] have reported some works in this field such as supramolecular microtubule [5] and coordination complex microtubes, [6] in which the linkers used are all limited in the multi-pyridyl-based molecules and the scale of the tubes are all in micrometer ranges.

Recently，M. E. Boom et al [11] and Qian et al [12] synthesized amorphous coordination complex nanotubes from $[PdCl_2(PhCN)_2]$ or Hg ions and multidentate ligand，[13, 14] but the linker they used still limited in the multi-pyridyl-based molecules. In addition to these pioneering reports, coordination complex nanotubes (CCNTs) are ultimate rare and the non-pyridyl-based coordination complex nanotubes have not been reported yet up to date. Even more so, the biomolecule-based coordination complex nanotubes (BMB-CCNTs) are still the unexploited area, but it was predicted being full of promising area for novel functional materials and life science. So, it is urgent needed to exploit the facile construction method to meet the increasing demand to creating novel functional materials. Herein, we report a kind of novel Ni-folate BMB-CCNTs with the inner diameter of 5~8 nm, fabricated by using biological active molecule folic acid (FA) and N_2H_4 (HZ) as a linker and nickel as a connector in a large scale. It is not only the first example of CCNTs formed by using non-pyridyl-based molecule as a linker, but also the first report on BMB-CCNTs. As we are well known, folic acid is a biocompatible, poorly immunogenic and tumor-specific molecule for a large fraction of human cancer cells with over-expressed folate receptor (FR), therefore, folic acid-based BMB-CCNTs can automatically aim against cancer cells and enter into the cytoplasm via FR-mediated endocytosis. More importantly, it overcomes the main limitation of antibody-drug conjugate as the targeting deliver system, i.e. the conjugate may be highly immunogenic, and thus lead to an antibody response against the conjugate, thereby precluding further use. [15] Another remarkable feature of the BMB-CCNTs reported here is no need to do any further completed and tedious post treatment to get targetable and biocompatible, [16, 17] which is beneficial to product in large scale. Furthermore, the novel BMB-CCNTs are also quite different

from the previous reported folate-drug conjugates, [18] i.e. it has a big enough empty cavity to load a dose of drug, therefore, it are small overcomes two main limitations of the folate-drug conjugate : 1) the dose deliverable is small, i.e. one molecule of drug for each molecule of folate; 2) the majority of the folate-drug complexes are small and as such are excreted in kidneys and re-absorbed in the proximal tubules, then leading to undesirable accumulation of folate-drug complexes in the kidney. It is full of promise smart multi-functional nanomedicine system. Especially, it was reported recently that human cancer is composed of a mixed population of malignant cells that carry multiple genetic mutations and it is almost impossible to treat cancer with a single therapeutic agent. [19-21] It is a big challenge to exploit a multifunctional therapeutic system. BMB-CCNTs reported here show a great promise for creating novel smart multi-functional nanomedicine system, and at same time, are a significant valuable to fundamental studies of CCNTs.

Characterization

TEM and energy-dispersive X-ray spectra (EDS) were performed on a JEOL 2100 with accelerating voltage of 200 kV. TEM samples were prepared by drop-casting dispersion onto copper grids covered by carbon film. Magnetic property measurements were performed using a Quantum Design MPMS XL-7 SQUID. SEM was performed on a JEOL S-4800 with accelerating voltage of 15 kV. The noncrystalline structure of the prepared CCNTs was identified by XRD with a Bruker D8 diffractometer system using a Cu Kα radiation source (λ = 0.15406 nm). Ultraviolet-visible spectra were collected using a LAMBDA-35 spectrometer. Infrared spectra (4000-400 cm^{-1}) were recorded on Bruker FTIR using KBr pellets. An inductively coupled plasma emission spectrometer was used to analyze the metal elements in the sample. MALDI-TOF mass spectra were collected using a LCQ mass spectrometer. XPS analysis was performed with a Physical Electronics Instruments ESCALB MK-II. The source was monochromatic Mg Kα radiation. The peak positions were referenced with respect to the C1s peak at 284.6 eV obtained from trace hydrocarbon contaminants in the samples. The survey spectra were run in the binding energy range 0-1000 eV, followed by high-resolution spectra of the C1s, N1s, O1s, and Ni2p regions. The EXAFS measurements at the Ni-K edge (8333 eV) were carried out in transmission mode at the U7C beamline at the National Synchrotron Radiation Laboratory in China (see Supporting Information for details). Confocal laser scanning microscope (CLSM) images were performed on CarlZeiss LSM 710 confocal laser scanning microscope. Flow cytometric analysis was performed on Becton-Dickinson FACS Calibur flow cytometry.

Preparation of Ni-folate BMB-CCNTs

In a typical experiment, folic acid (0.5 mmol) and $NiCl_2$•$6H_2O$ (1 mmol) were added to a mixture of ethanol (3 ml) and H_2O (12 ml) with stirring and ultrasonicated for 10 min, followed by addition of aqueous hydrazine (10 ml, 85%) with continuous stirring (pH = 10.5). The mixture immediately became slurry, was transferred to a poly-tetrafluoroethylene-lined autoclave with heating at 120 °C for 12 h, and then cooled naturally to room temperature. The crude sediment was washed several times with water and ethanol. Then it was first dialyzed against an aqueous solution of PBS (pH 7.4) and then against de-ionized water in a dialysis tube (MWCO: 3500). The aqueous solution of pure BMB-CCNTs was lyophilized to obtain the brown sample for the following characterization. Yield 90 %.

Preparation of Ni-Folate in NH_3·H_2O and Ni- Folate in NaOH as the control experiments

In this case, the nickel folate coordination complex was prepared by solvothermal procedure without hydrazine, that is, by adding ammonia aqueous solution or NaOH to adjust the pH of the reaction solution to same as that of the hydrazine condition. In a typical reaction, folic acid (0.5 mmol) and $NiCl_2$·$6H_2O$ (1 mmol) were added to the mixture of ethanol (3 ml) and H_2O (12 ml) with stirring and ultrasonicated for 10 min, followed by addition of NaOH (0.1 M) or ammonia aqueous solution (25 %) with continuous stirring (pH = 10.5). The mixture was transferred to the poly-tetrafluoroethylene lined autoclave, heated at 120 °C for 12 h, then cooled naturally to room temperature. The crude sediment was washed several times with water and ethanol. Then it was first dialyzed against an aqueous solution of PBS (pH 7.4) and then against de-ionized water in a dialysis tube (MWCO: 3500). The aqueous solution of pure BMB-CCNTs was lyophilized to obtain the brown sample for the following characterization. Yield 90 %.

Preparation of cisplatin loaded Ni-folate BMB-CCNTs (CDDP-CCNTs)

20 ml of Ni-folate BMB-CCNTs (2 mg mL^{-1}) were added to 20 mL of 2.5 mg mL^{-1} cisplatin solution and the mixture was kept in a shaker for 24 h in dark conditions. Finally, the cisplatin loaded BMB-CCNTs (CDDP-CCNTs) were washed five times with Milli-Q water to remove unbound drug molecules. The supernatant was collected to determine the drug encapsulation efficiency (EE) by ICP.

Cytotoxicity assay

Cell cytotoxicity of blank BMB-CCNTs, CDDP-CCNTs , CDDP or free folic acid were evaluated by MTT assay using human cervical cancer HeLa cells(over express of FR), human lung adenocarcinoma A549 cells(low express of FR) and normal human embryonic lung fibroblasts HELF cells(low express of FR) with the different express level of folate receptor . Samples containing 2×10^4 cells in 100 μL DMEM containing 10% PBS were plated in 96-well plates and incubated for 24 h at 37 °C in humanized atmosphere containing 5% CO_2. These cells were respectively incubated with different concentration solutions of blank BMB-CCNTs, CDDP-CCNTs, free cisplatin or free folic acid for 96 h under same condition. After incubation, 20 μL MTT (5 mg mL^{-1}, dissolved in PBS, pH 7.4) was added to each well and incubated for another 4 h. Then removed the incubated medium, added 150 μL DMSO to each well and gently shook for 10 min at room temperature. Absorbance was measured at 490 nm using a Spectramax M5 Microtiter Plate Luminometer (Molecular Devices, US). Set the absorbance value of untreated cells to be 100%. The concentration of paclitaxel at which inhibited 50% cell growth compared with untreated cells (IC_{50}), was defined by curve fitting (LOGIT method) using SPSS software. Each experiment was repeated three times in triplicate

(n = 9).

Bio-TEM observations for HeLa Cells

The HeLa cells were incubated with 25 μg mL^{-1} CDDP-CCNTs in DMEM medium in 5% CO_2 at 37°C for 24 h. Afterwards, cells were washed three times with PBS and subsequently fixed with 2.5% glutaraldehyde in 0.03 M potassium phosphate buffer. Cells were then washed with PBS, postfixed with 1% osmium tetroxide in sodium carboxylate buffer, washed with 0.05 mol L^{-1} maleate, and stained with 0.5% uranylacetate (Sigma Aldrich) in maleate buffer. After washing the cells in 0.05 mol L^{-1} maleate, the cells were dehydrated in a grading series of ethanol followed by acetone, embedded in Epon, and dried in an oven at 60 °C for 4 days. Ultrathin sections of approximately 50 nm thick were cut with a diamond knife on a Leica ultracut R ultramicrotome and transferred to the copper grid. The images were viewed on JEOL-2100 electron microscopy.

The confocal laser scanning microscope (CLSM) images

HeLa or HELF cells were seeded on glass coverslips in single well plates at a density of 1×10^5 cells/well. After complete adhesion, the cells were washed 3 times with growth media and incubated at 37 °C in 5% CO_2 for 24 h with the FITC-labelled CDDP-CCNTs. Dual fluorescence-labelling experiments were performed and the cells with dual colours, green for cytoplasm and blue for nucleus, were visualized to further determine the intracellular distribution of CDDP-CCNTs more precisely.

Results and Discussion

Characterization

Ni-folate BMB-CCNTs with uniform diameter were synthesized by the solvothermal method (Scheme 1) and is stable in air, and insoluble in common organic solvents.

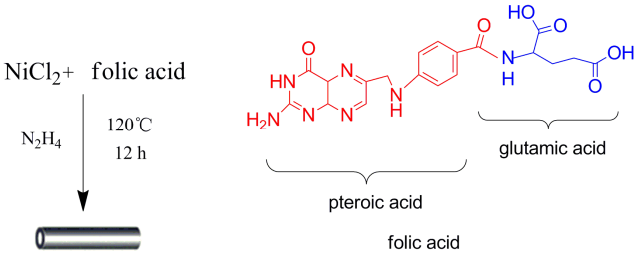

Scheme 1 Preparation of nano-sized Ni-folate BMB-CCNTs.

SEM and TEM images of Ni-folate BMB-CCNT (Fig. 1) show homogeneous nanotubes with an outer diameter of 16-20 nm and length of 50-300 nm. A clear open end of the nanotube can be observed in SEM image (Fig. 1a). And the most of nanotubes aggregated to form tube bundle as observed in Fig. 1b due to the Van der vaals interaction. TEM image in Fig. 1c clearly exhibits the fine morphologies of several individual nanotubes, and the magnification TEM image of the BMB-CCNTs in Fig. 1d shows its smooth surface and hollow structure with 5-8 nm for inner diameter and 4-7 nm wall thickness. The inset SAED in Fig. 1d indicates the non-crystalline nature of the nanotubes, which is accordance with the results from X-ray powder diffraction (see ESI Fig. S1).

The chemical composition of the BMB-CCNTs was determined by energy dispersive X-ray (EDX) spectroscopy, elemental analysis (EA) and Inductively Coupled Plasma (ICP) emission spectrum. Based on these results, the formula of $[Ni_2(FA)(N_2H_4)_3(H_2O)_2(OH^-)_2]$ is suggested. According to the formula, elemental composition calculated (C, 31.55 wt %; H, 4.84 wt %; N, 25.18 w %; and Ni, 16.24 wt %, with a molecular weight of 722.7) is good agreement with experimental data (C: 32.24 wt %; H: 4.85 wt %; N: 24.64 wt % and Ni: 16.72 wt %). The molecular ion peak of the nanotube in matrix-assisted laser desorption/ionization time-of-flight mass spectroscopy (MALDI-TOF) located at 745.6, which is attributed to $[M+Na]^+$ measured in the positive mode, that is, $[Ni_2(FA)(N_2H_4)_3(H_2O)_2(OH^-)_2]$+Na.

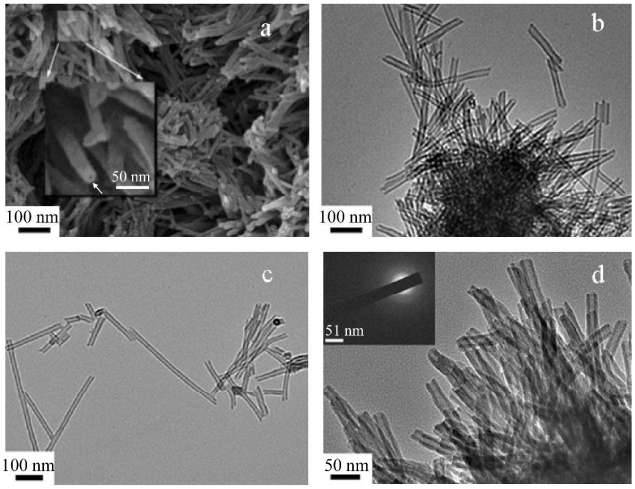

Fig.1 (a) SEM image (the inset is high-magnification image) and (b) TEM image of the tube bundle showing many open ends. (c) TEM image of some individual nanotubes (d) The magnification TEM image of BMB-CCNTs (the inset is the SAED pattern of the tube showing its non-crystalline nature)

X-ray photoelectron spectroscopy (XPS) studies were performed to further investigate the composition of the BMB-CCNTs and the valence state of the elements in it (Fig. 2). The results show that all Ni in the sample are Ni (II) with the characteristic core level peak of Ni 2p1/2 and Ni 2p3/2 near 855.2 eV and 873.1 eV (Fig. 2a), within the Ni 2p peak range, compared with other known Ni (II) compounds. [22-24] All C1s spectra show peaks close to the expected binding energies of 285.7, 286.8, and 288.8 eV (Fig. 2b), and are attributed to C-C (or C-H), C=O(or C-N), and O-C=O in the folic acid backbone, respectively. [25, 26] The N1s band is deconvoluted into four bands at 399.6, 400.4, 401.1, and 401.6 eV (Fig. 2c). To ascribe the N from the coordinated hydrazine, we synthesized the Ni (II) complex with hydrazine according to a previous report. [27] The inset in Fig. 2c is the N1s band of complex $Ni(N_2H_4)_nCl_2$(n = 2 or 3), showing a single sharp peak at 400.2 eV attributed to N-Ni; this value is similar to the value for the quaternary N in the literature. [28] Based on these results, the N1s peak at 400.4 eV in the XPS of the Ni-FA-HZ CCNTs may be attributed to N-Ni, confirming the coordination of N_2H_4 with Ni (II). The other three peaks are mainly attributed to the amine N or pterin N from the folic moiety. [29] Via peak deconvolution of the O1s peak (Fig. 2d), the oxygen state was established. The O1s peak was

deconvoluted into four contributions. A distinction was made between amide carbonyl O (531.6 eV) and carboxylate O (C=O 532.1 eV and C-O 532.5 eV). Compared with the free carboxylate group, in which the O1s BE difference of C=O and C-OH was more than 1.5 eV, [30, 31] the corresponding small difference of 0.4 eV in CCNTs provided evidence for chelating coordination of carboxylate groups because two oxygen atoms in the carboxylate group all coordinated to the Ni (II) center, making the electrons more delocalized around them and therefore reducing the BE difference. The contribution at 533.2 eV corresponded to the oxygen in hydroxyl groups and water molecules. [26, 32]

The ultraviolet-visible-near-infrared (UV-Vis-NIR) diffuse reflection spectrum of the BMB-CCNTs (ESI Fig. S2) and IR spectra (ESI Table S1) further evidence that Ni (II) exists in an octahedral coordination, where –COO group is bidentated coordinated to Ni^{2+} ion. There are two new bands at 983 cm^{-1} and 940 cm^{-1} in the CCNTs sample. The former can be attributed to ν (N-N) in unidentate coordination NH_2-NH_2 and the latter to ν (N–N) in bridging mode NH_2-NH_2, providing further evidence of N_2H_4 coordinating to Ni. [33]

Based on the above results from element analysis, XPS, UV-Vis and FT-IR spectroscopes, we may conjecture that the reasonable structure of Ni folate in the BMB-CCNTs is the six coordination octahedron with four O atoms and two N atoms.

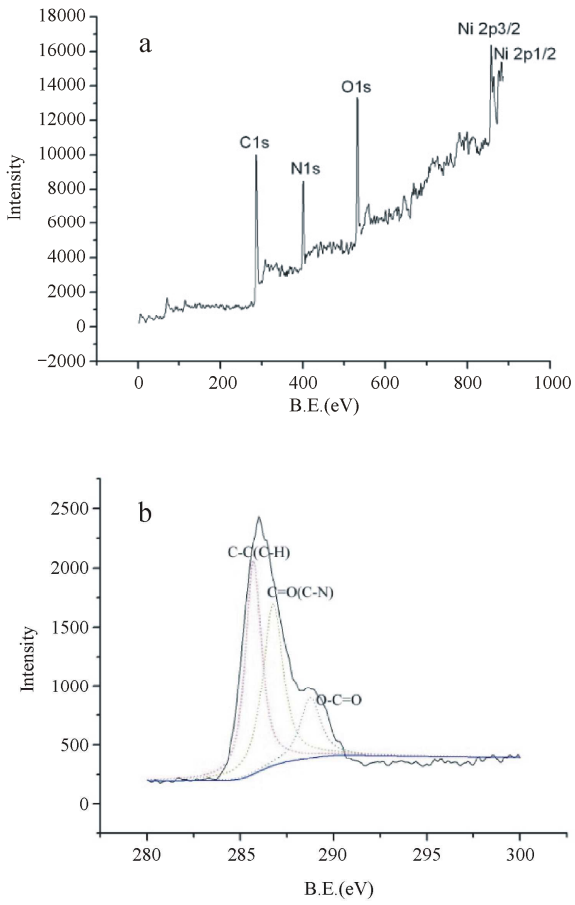

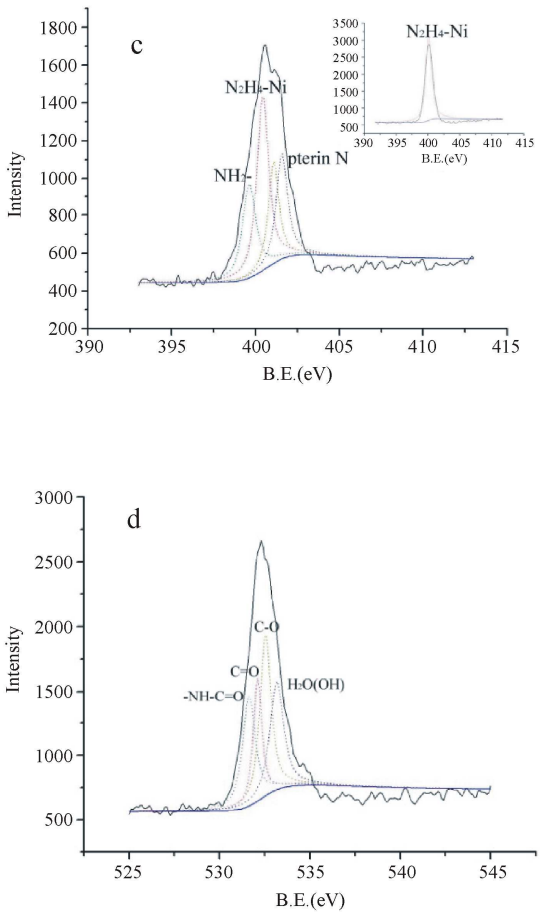

Fig.2 XPS spectra of BMB-CCNTs: (a) full scan, (b) C1s, (c) N1s (inset: N1s of Ni-hydrazine complex), and (d) O1s.

Due to the non-crystalline character of the BMB-CCNTs, X-ray diffraction analysis method is unusable for its structure studies, but the extended X-ray absorption fine structure (EXAFS) analysis is the most powerful means for non-crystalline materials. Ni K-edge X-ray absorption spectroscopic measurements were conducted for Ni folate complexes (Ni-FA) and Ni-folate BMB-CCNTs (see ESI Fig. S3 - S5 and Table S2 for details). The extracted structural parameters are summarized in Table 1. The fitting values of $Ni(acac)_2 \cdot 2H_2O$ were used as a judging standard to inspect the rationality of our EXAFS data and processing procedures. The experimental data of Ni folate BMB-CCNTs fit well to the six coordination mode with two nitrogen atoms located at 2.09 Å and four oxygen atoms at 2.04 Å around Ni (II). The values of Ni-O and Ni-N bond lengths are in a reasonable range. [34] All of the results we've got prove that the coordination structure of the Ni^{2+} ion in CCNTs is a six coordination octahedron with four oxygen atoms and two nitrogen atoms.

Table 1. Local structural fitting parameters of the Ni-O and Ni-N shells around Ni in Ni-FA, Ni-folate BMB-CCNTs and $Ni(acac)_2•2H_2O$

Sample	Shell	R	N	S_0^2	ΔE_0	σ^2
Ni-FA	Ni-O	2.03	6.0	0.90	3.82	0.0071
Ni-folate BMB-CCNTs	Ni-O	2.04	4.0	0.90	3.63	0.0065
	Ni-N	2.09	2.0	0.90	3.90	0.0077
$Ni(acac)_2•2H_2O$	Ni-O[a]	1.99	4.0	0.90	1.70	0.0054
	Ni-O[b]	2.10	2.0	0.90	1.34	0.0099

[a] four oxygen atoms in the equatorial plane; [b] two oxygen atoms located at the axial position

Mechanism of nanotube formation

TEM images at different times (Fig. 3) were used to trace the reaction process. TEM image of the product reacted for 20 min. shows a big nanosheet (300-400 nm in width and 500-1000 nm in length) with the edge curled (Fig. 3a). After reacted for 1.5 h, many perfect nanotubes were formed (Fig. 3b), but some tubular structures, which have not yet stripped from the mother nanosheets completely, still were remained. This observation provides firm evidence that the precursor of the nanotube is nanosheet. After reacted for 2 h, the nanosheets disappear and transform into regular nanotubes (Fig. 3c). Based on the Van der waals interaction between the adjacent nanotubes, the individual tubes will aggregate into a nanotube bundle as the reaction time lasting (Fig. 3d).

To understand the role played by hydrazine, nickel folate complex pre-prepared is treated under solvothermal conditions (120 °C), using $NH_3·H_2O$ or NaOH instead of hydrazine. The TEM image (Fig. 4a) of the sample prepared in the case of $NH_3·H_2O$ as the base shows that the products appear as the spherical-like structures, while the products treated with NaOH under the same solvothermal conditions present as the nanosheets with the curled edge (Fig. 4b).These experimental results demonstrate that hydrazine plays a decisive role in the formation of nanotubes from the Ni-FA complex via nanosheets to final nanotubes. The nanotube is hard to be formed without the bridging ligand hydrazine.

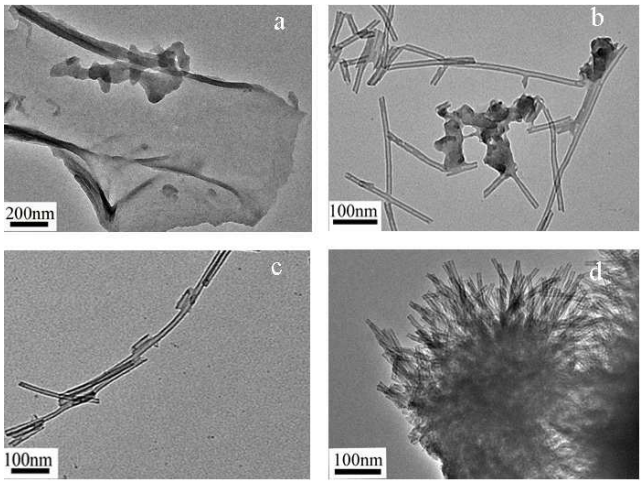

Fig.3 TEM images of products collected at various reaction times: (a) 20 min, (b) 1.5 h, (c) 2 h, and (d) 12 h.

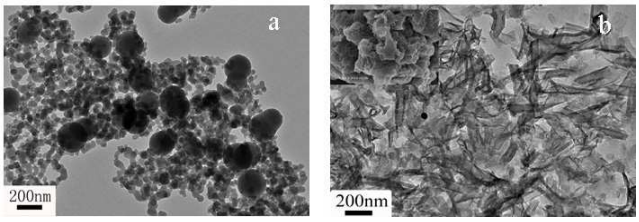

Fig.4 TEM images of (a) the obtained coordination complex from NiCl2 and folic acid treated with $NH_3·H_2O$ for 12 h and (b) the Ni-folate coordination complex treated with NaOH for 12 h (the inset is an SEM image).

As is well known, folic acid is composed of pteroic acid and glutamic acid connected via amido bond (Scheme 2), and the unit of pteroic acid in the folic acid can connect together via hydrogen bond to form a tape-like structure as shown in Scheme 2a. The glutamic acid unit in folic acid would react with Ni^{2+} forming a coordination complex, which does not hinder the hydrogen bonds among the pteroic acid units from forming, therefore, Ni-FA complexes appear a tape-like structure as shown in Scheme 2a. Hydrazine acts as a bridge ligand coordinating to two Ni ions in the neighbouring tape to form a wide nanosheet (Scheme 2b). The nanosheet may curl via adjusting the relative orientation to the rigidity aromatic ring frame. The high reaction temperature aggravates the intermolecular relatively movement in the nanosheet under solvothermal conditions, which promotes the nanosheet curling to minimize its surface free energy (Scheme 2c) and further to form nanotubes via partial initial bond broken and new bond formed. It seems that the hydrazine behaves like a molecular "thread" sewing the Ni-FA complex nanocloth into nanotubes. The Ni-folate nanotube synthesized here is the first example of non-pyridyl-based coordination complex nanotube up to date. Scheme 2d shows the possible structure unit of the CCNTs.

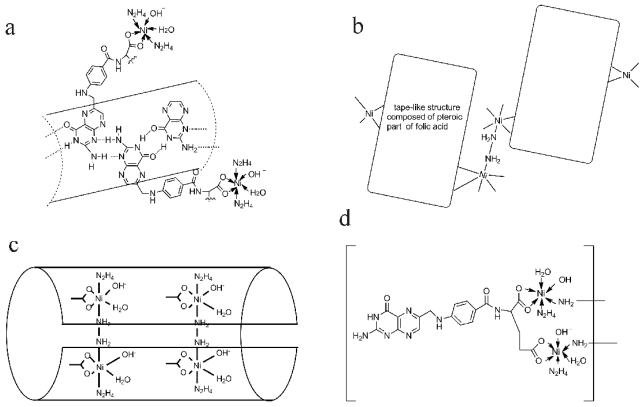

Scheme 2 Formation of Ni-folate BMB-CCNTs

In vitro cytotoxicity and cellular uptake of CDDP-CCNTs

As a potent drug carrier, cisplatin (CDDP) was loaded into the Ni-folate BMB-CCNTs to get CDDP-CCNTs. In order to inspect antitumor activity and drug targeting delivery function of Ni-folate BMB-CCNTs, human cervical cancer HeLa cells, human lung adenocarcinoma A549 cells and human normal human embryonic lung fibroblasts HELF cells were treated with Ni folate BMB-CCNTs and CDDP-CCNTs for 96 h. The cells

incubated with CDDP or FA were used as the control groups and the cell viability was determined by MTT (3-[4,5-dimethylthiazol-2-yl]-2,5-diphenyl tetrazolium bromide) assay. The results show that Ni-folate BMB-CCNTs own exhibit high antitumor activity (IC_{50} of HeLa is 0.586 ug mL^{-1}, IC_{50} of A549 is 0.855 ug mL^{-1}, IC_{50} of HELF is 10.139 ug mL^{-1}) which is almost same as CDDP (IC_{50} of HeLa is 0.464 ug mL^{-1}) and is a potent nanomedicine, while its cytotoxicity for normal cell is less than the CDDP (IC_{50} of HeLa is 0.464 ug mL^{-1}, IC_{50} of HELF is 2.724 ug mL^{-1}). By comparison, FA either in solid nanosheet structure or in aqueous solution shows no inhibition activity. It is exciting that the biomolecule-based nanomaterial bearing the potent anticancer activity of its own has rarely been reported up to date.

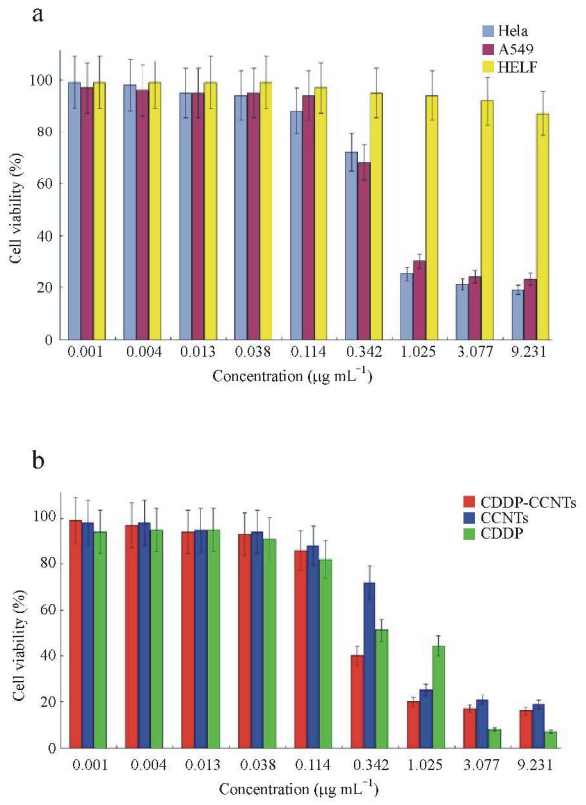

Fig.5 (a) Cell viability of HeLa cell lines (blue), A549 cell lines (violet) and HELF cell lines (yellow) after co-incubation with BMB-CCNTs respectively, for 96 h and (b) Cell viability of HeLa cell lines after co-incubation with CDDP-CCNTs (red), CCNTs (blue) and CDDP (green) respectively, for 96 h.

After loaded with a dose of CDDP as model drug (The final drug entrapment efficiency was 45.5%, wherein the amount of CDDP loaded is 36.2% by weight of Pt), CDDP-CCNTs inhibit the tumor cell growth effectively as expected (IC_{50} of HeLa is 0.305 ug mL^{-1}, IC_{50} of A549 is 0.796 ug mL^{-1} and IC_{50} of HELF is 6.828 ug mL^{-1}). As we can see from Fig. 5a, the Ni-folate BMB-CCNTs show the specific targeting effect toward the HeLa cells with over expression of FR, compared with the cells with lower expression of FR such as A549 cells and the human normal HELF cells. The folic acid as the main component of nanotubes promotes CDDP-CCNTs the internalization in FR (+) cells. The extra efficacy may be partially attributed to the increase accumulation of the drug in tumor cells due to specific target delivery function and partially to a synergetic effect of two drugs: Ni-folate BMB-CCNTs and CDDP (Fig. 5b). These results reveal that the biomolecule-based nanotubes would be full of smart multi-functional nanomedicine system.

Bio-TEM, fluorescence and dual fluorescence-labeling Ni folate BMB-CCNTs were conducted to inspect whether the CDDP-CCNTs were internalized in HeLa cells. Fig. 6a shows the image of the HeLa cell alone without CDDP-CCNTs for comparison. In Fig. 6b, some aggregates can be seen as black clusters near the cell membrane (the right region marked with red rectangle), and some of them are distributed in the cytoplasm (the left region marked with red ellipse). Fig. 6c and 6d are the magnified images of the corresponding region marked in Fig. 6b. It shows that most of the nanotubes are degenerated into nano pieces, but a few of nanotubes still remain (red arrow in Fig. 6d). Furthermore, in another cell, almost all the nanotubes transform to the nano pieces. The reason for this might be relative to the acidic environment in the tumor cell. After entering into tumor cell via FR-mediated endocytosis, nanotubes suffer from a corrosion of the acid and gradually collapse and break up to smaller pieces, which is favour the drug release in the target site. In order to confirm our conjecture, we conduct the further studies, that is, soaking the original BMB-CCNTs into the PBS solution with pH=6.5 for 6 hr, which simulates the pH condition[35] during the process of incubation CCNTs with HeLa cells. The results show that the nanotubes really appear acid corrosion. Compared to the original CCNTs clusters (Fig. 6e), the open ends of the nanotubes disappear and break up to the pieces (in Fig 6f), on the contrary, the nanotubes maintain their original tubular structure when being immersed into the solution with pH=7.4. It means that the structure stability of the nanotubes is pH dependent and that it is stable in vivo until entering into tumor cell, which is required for an effective drug carrier. The more behaviors of controlled drug release and CCNTs metabolism research is undergoing.

To further evidence the CDDP-CCNTs were internalized in HeLa cells, rather than bound to the cell surface, we used fluorescein isothiocyanate (FITC) as a marker to follow the movement of the CDDP-CCNTs after 24 h incubation with HeLa cells. The resulting FITC-labelled CDDP-CCNTs were washed repeatedly to remove any unbound FITC molecules. The confocal laser scanning microscope (CLSM) images of the Hela cells treated by 50 μg mL^{-1} FITC-labelled CDDP-CCNTs after 24 h showed apparent green fluorescence (Fig. 7a). In comparison, the HELF cells treated under the completely same conditions showed extremely weak fluorescence (Fig. 7b). The results suggest that the CDDP-CCNTs could easily bind to the tumor cells that over-expressed folate receptor with its targeting delivery capacity, and then enter into the cytoplasm. However, CDDP-CCNTs are not inclined to bind with the normal cells, resulting in more inefficiently taken up into the HELF cells. In order to quantify the positive/negative ratio based on average FITC fluorescence signal/intensity to find out the specificity/selectivity of the folate-based targeting system, flow cytometric analysis of CDDP-CCNTs in HeLa and HELF cell lines was carried out. The results in Fig. 7c and Fig. 7d showed that CDDP-CCNTs were taken into HeLa cell lines at about 98.6% and HELF cells lines at about 34.1% for comparison.

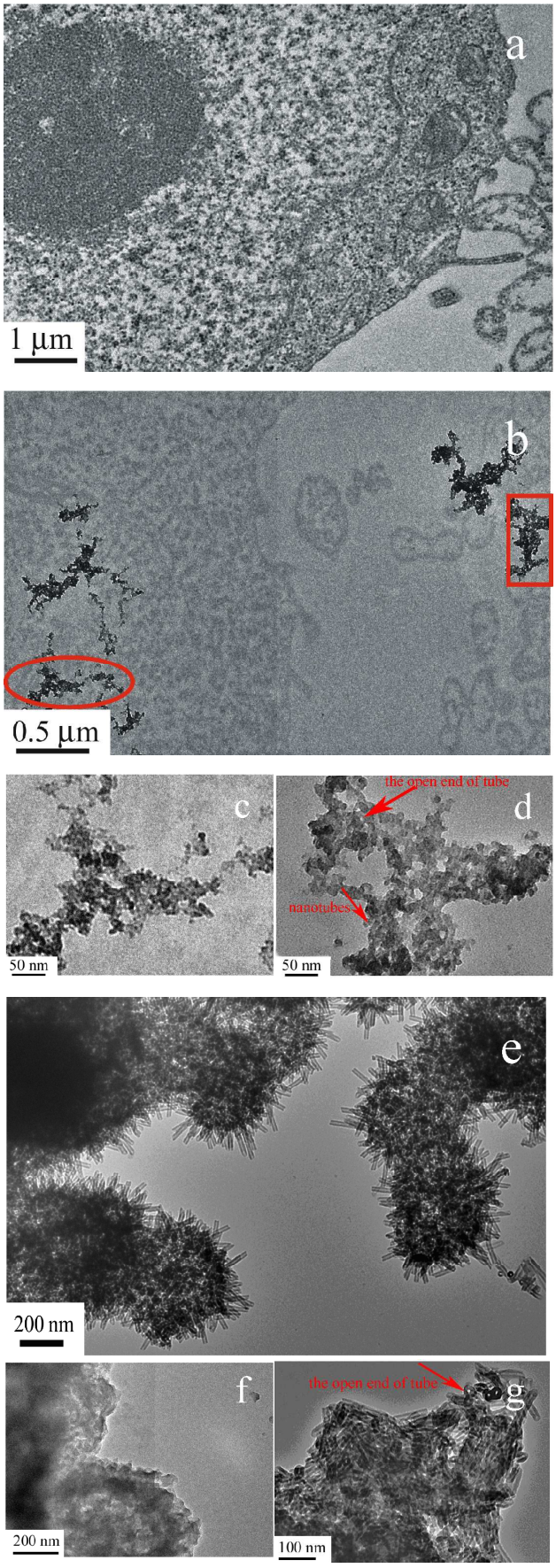

Fig.6 Bio-TEM images to show the process of BMB-CCNTs being uptaken by HeLa cell: (a) normal HeLa cells without CDDP-CCNTs, (b) cells treated with 25 μg mL^{-1} CDDP-CCNTs for 6 h: the nano-clusters are near the cell membrane and dispersed in the cytoplasm, (c) enlarged view of the cell cytoplasm region marked with red ellipse, (d) enlarged view of the cell membrane region marked with rectangle.
To confirm the transformation of nanotubes in the acidic condition, CCNTs are soaked in the PBS solution for comparison: (e) the overview of the perfect nanotubes clusters prepared by the solvothermal method, (f) nanotubes are transformed at pH=6.5, (g) nanotubes are maintained at pH=7.4.

Combined with the result of the Bio-TEM above mentioned, we deduce that lots of CDDP-CCNTs are entering into the cytoplasm through endocytosis, thus producing the apparent and inhomogeneous green fluorescence around the nucleus. CCNTs collapsed and broke up into nano pieces, at the same time, released CDDP in HeLa cell and the latter one entered into cell nucleus to complete the drug delivery process. The exact antitumor mechanism is no clear yet, and a further study is needed. The possible delivery process of CDDP-CCNTs drug delivery system is depicted in Fig. 8.

Conclusion

In summary, a simple chemical approach was developed for the synthesis of BMB-CCNTs via H bonds and coordination bonds. Hydrazine behaves as a molecular "thread" sewing the coordinate complex nanosheet of the Ni-folate into nanotubes with an inner diameter of 5-8 nm. Based on the experimental results, a three-stage formation mechanism is proposed. This work provides firm experimental evidence for the formation of CCNTs via curling of coordination complex nanosheets. It is not only the first example of CCNTs formed by using non-pyridyl-based molecule as a linker, but also is the first report on BMB-CCNTs with anticancer activity. Compared with previous works in the literature, [36] this work has following remarkable features: (1) the BMB-CCNNTs is no need to do further post treatment to get targeting deliverable and biocompatible performance, which is of beneficial to produce in large scale; (2) it overcomes the main limitations of antibody-drug and folate-drug conjugates, which is convenient for application in production and therapy; (3) the tubular structure of CCNTs offers a big enough hollow cavity to fill a dose of various drug molecules to reduce the generation of the drug-resistance cancer cells; (4) the nanotubes is stable enough until entering into tumor cell and collapse into nano pieces to release drug in tumor cell; (5) the skeleton composed of FA gives a target delivery function to this novel drug delivery system. The results of cytotoxicity and cellular uptake of CDDP-CCNTs in vitro exhibit that Ni-folate BMB-CCNTs can easily enter into the tumor cell via folate receptor-mediated endocytosis, combined with the synergism, significantly increase the antitumor efficacy of CDDP-CCNTs. This work provides enlightenment for creating a novel multi-functional nanomedicine system, which

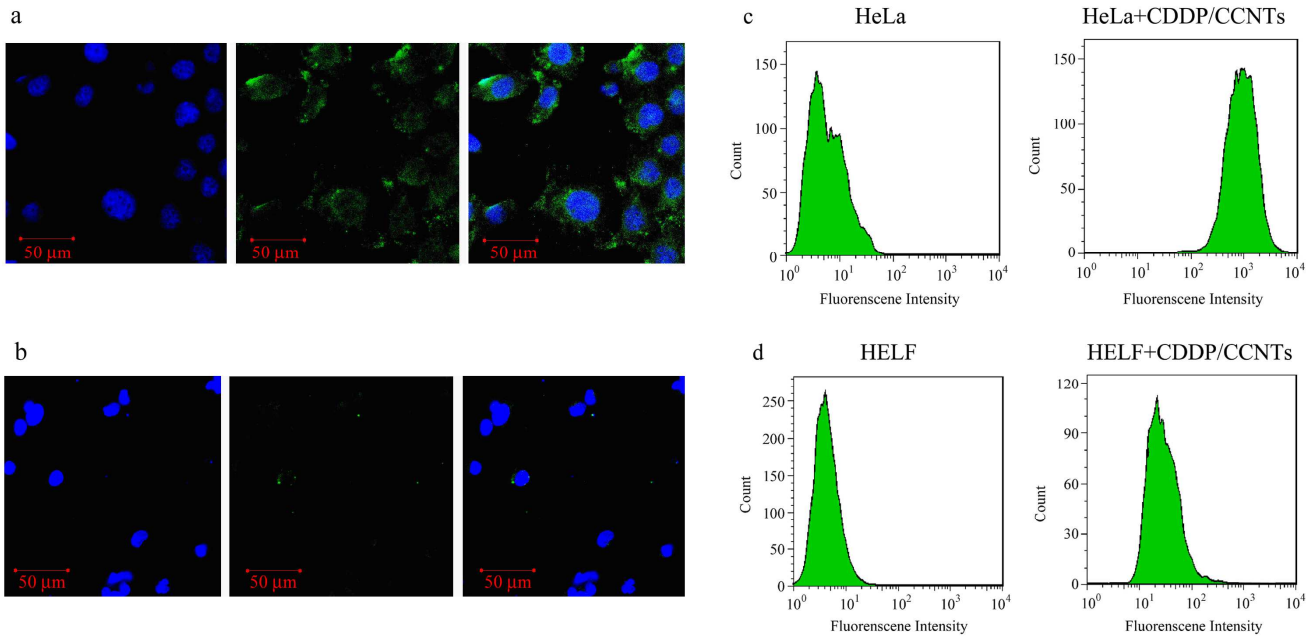

Fig.7 Confocal laser scanning microscope images (the left:: the blue nucleus stained by DAPI collected at 360 nm, middle: collected at 530 nm for FITC channel, right: merge images) of (a) HeLa cells images and (b) HELF cells images after treating 50 μg mL^{-1} of FITC-labelled CDDP-CCNTs for 24 h. (c) Flow cytometric analysis of CDDP-CCNTs in HeLa cell lines (left: HeLa cell lines without CDDP-CCNTs for control). (d) Flow cytometric analysis of CDDP-CCNTs in HELF cell lines (left: HELF cell lines without CDDP-CCNTs for control). CDDP-CCNTs were taken into HeLa cell lines at about 98.6% and HELF cells lines at about 34.1% for comparison.

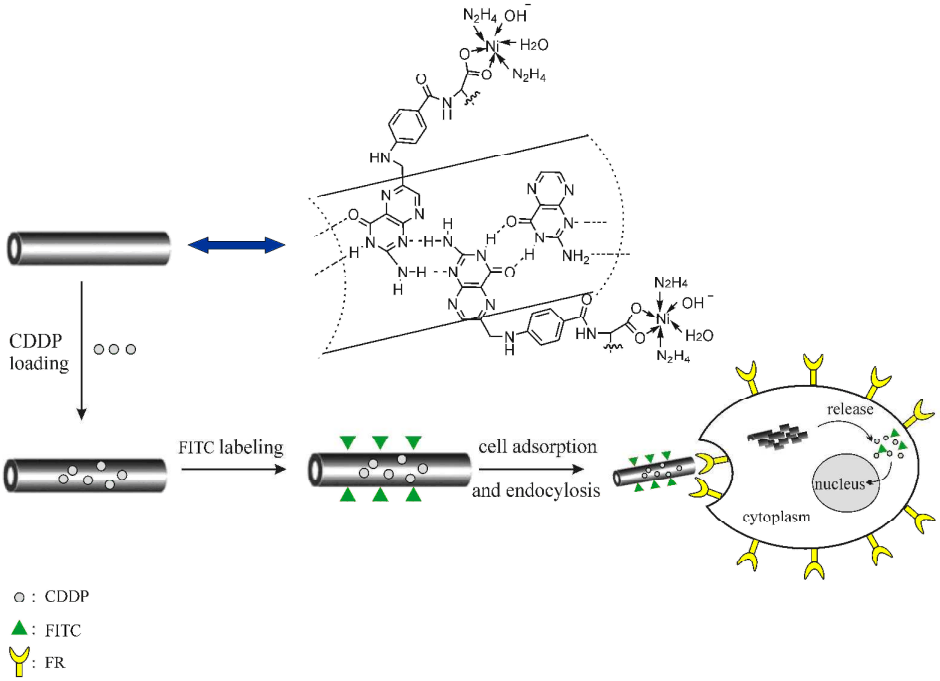

Fig.8 Schematic representation of CDDP-CCNTs drug delivery system

may act as a target seeker and can concomitantly kill multiple malignant cells with better efficacy and less toxic-side effect.

Acknowledgements

Thanks for financial support from National Major Basic Research Program (973 program 2007CB936302) and the National Natural Science Foundation of China under major project No.90606005, and for help in EXAFS experiments from the National Synchrotron Radiation Laboratory in China. This study was also sponsored by the National Natural Science Foundation of China (No. 21401216) and Qing Lan Project in Jiangsu Province.

Notes and references

[a] State Key Laboratory of Coordination Chemistry, School of Chemistry and Chemical Engineering, Nanjing University, Nanjing, P.R., China. E-mail: zhengxu@nju.edu.cn

[b] State Key Laboratory of Natural Medicines, School of Sciences, China Pharmaceutical University, Nanjing, P.R., China. E-mail: zwy_1115 @ 126.com

Electronic Supplementary Information (ESI) available: [X-ray powder diffraction, the ultraviolet-visible-near-infrared (UV-Vis-NIR) diffuse reflection spectrum, IR spectra and the extended X-ray absorption fine structure (EXAFS)]. See DOI: 10.1039/b000000x/

1 E. Breynaert, J. Emmerich, D. Mustafa, S. R. Bajpe, T. Altantzis, K.V. Havenbergh, F. Taulelle, S. Bals, G. V. Tendeloo, C. E. A. Kirschhock and J. A. Martens, *Adv Mater.*, 2014, *30*, 5173-5178.

2 L. Heinke, Z. G. Gu and C. Wöll, *Nat Commun.*, 2014, *5*, 4562-4568.

3 Y. Lu, B. Yan and J. L. Liu, *Chem. Commun.,* 2014, *50*, 9969-9972.

4 W. L. Leong and J. J. Vittal, *Chem. Rev.*, 2011, *111*, 688-764.

5 N. E. Shi, G. Yin, H. B. Li, M. Han and Z. Xu, *New J. Chem.*, 2008, *32*, 2011-2015.

6 N. E. Shi, G. Yin, X. W.Wei and Z. Xu, *Carbon*, 2009, *47*, 534-538.

7 A. Facchetti, *Angew. Chem. Int. Ed.*, 2011, *50*, 6001-6003.

8 S. Zhang, S. Yang, J. Lan, S. Yang and J. You, *Chem. Commun.*, 2008, *52*, 6170-6172.

9 S. D. Weitman, R. H. Lark, L. R. Coney, D. W. Fort, V. Frasca, V. R. Zurawski and B. A. Kamen, *Cancer Res.*, 1992, *52*, 3396-3401.

10 S. Wang and P. S. Low, *J. Control Release*, 1998, *53*, 39-48.

11 A. H. Barak, G. Ruiter, M. Lahav, S. Sharma, O. Gidron, G. Evmenenko, P. Dutta, M. Bendikov and M. E. Boom, *Chem- Eur. J.*, 2013, *19*, 8821-8831.

12 C. F. Zhang, A. Liu, M. Chen, C. Nakamura, J. Miyake and D. J. Qian, *ACS Appl. Mater. Interfaces*, 2009, *1*, 1250-1258.

13 R. Kaminker, R. Popovitz-Biro and M. E. Boom, *Angew. Chem. Int. Ed.*, 2011, *50*, 3224-3226.

14 B. Liu, D. J. Qian, M. Chen, T. Wakayama, C. Nakamura and J. Miyake, *Chem. Commun.*, 2006, *30*, 3175-3177.

15 G. Henriksen, O. S. Bruland and R. H. Larsen, *Anticancer Res.*, 2005, *25*, 9-15.

16 C. P. Leamon, I. R. Vlahov, J. A. Reddy, M. Vetzel, H. K. R. Santhapuram, F. You, A. Bloomfield, R. Dorton, M. Nelson, P. Kleindl, J. F. Vaughn and E. Westrick, *Bioconjugate Chem.*, 2014, *25*, 560-568.

17 T. Zhang, F. Li, J. Yi, C. H. Gu, L. Fan, Y. B. Qiao, Y. C. Tao, C. Cheng and H. Wu, *Eur. J. Pharm. Sci*., 2011, *42*, 517-526.

18 R. Vlahov and C. P. Leamon, *Bioconjugate Chem.*, 2012, *23*, 1357-1369.

19 P. Fan, B. Shen, W. B. Bu, F. Chen, Q. J. He, K. L. Zhao, S. J. Zhang, L. P. Zhou, W. J. Peng, Q. F. Xiao, D. L. Ni, J. N. Liu and J. L. Shi, *Biomaterials,* 2014, *35*, 8992-9002.

20 H. F. Shen, J. You, G. D. Zhang, A. Ziemys, Q. P. Li, L. T. Bai, X. Y. Deng, D. R. Erm, X. W. Liu, C. Li and M. Ferrari, *Adv. Healthc Mater.*, 2012, *1*, 84-89.

21 C. M. Hu and L. Zhang, *Biochem. Pharmocol.*, 2012, *83*, 1104-1111.

22 L. Scudiero, D. E. Barlow and K. W. Hipps, *J. Phys. Chem. B*, 2000, *104*, 11899-11905.

23 D. H. Karweik and N. Winograd, *Inorg. Chem.*, 1976, *15,* 2336-2342.

24 C. Berríos, J. F. Marco, C. Gutiérrez and M. S. Ureta-Zañartu, *J. Phys. Chem. B*, 2008, *112*, 12644-12649.

25 C. J. P. Boonaert, Y. F. Dufrêne, S. R. Derclaye and P. G. Rouxhet, *Colloids Surf. B*, 2001, *22*, 171-182.

26 E. M. Marti, C. Methivier and C. M. Pradier, *Langmuir*, 2004, *20*, 10223-10230.

27 J. W. Park, E. H. Chae, S. H. Kim, J. H. Lee, J. W. Kim, S. M. Yoon and J. Y. Choi, *Mater. Chem. Phys.*, 2006, *97*, 371-378.

28 J. O. Hwang, J. S. Park, D. S. Choi, J. Y. Kim, S. H. Lee, K. E. Lee, Y. H. Kim, M. H. Song, S. Yoo and S. O. Kim, *ACS Nano*, 2012, *6,* 159-167.

29 K. Hayashi, K. Ono, H. Suzuki, M. Sawada, M. Moriya, W. Sakamoto and T. Yogo, *ACS Appl. Mater. Inter.*, 2010, *2*, 1903-1911.

30 A. J. Plomp, D. S. Su, K. P. Jong, J. H. Bitter, *J. Phys. Chem. C*, 2009, *113*, 9865-9869.

31 M. A. Fraga, E. Ordao, M. J. Mendes, M. M. A. Freitas, J. L. Faria and J. L. Figueiredo, *J. Catal.*, 2002, *209,* 355-364.

32 A. R. Slaughter and M. S. Banna, *J. Phys. Chem.*, 1988, *92*, 2165-2167.

33 J. W. Park, E. H. Chae, S. H. Kim, J. H. Lee, J. W. Kim, S. M. Yoon and J. Y. Choi , *Mater. Chem. Phys.*, 2006, *97*, 371-378.

34 Ö. Metin, L. T. Yıldırım and S. Özkar, *Inorg.Chem. Commun.*, 2007, *10,* 1121-1123.

35 B. B. Wang, C. V. Galliford and P. S. Low, *Nanomedicine*, 2014, *9*, 313-330.

36 J. Z. Du, X. J. Du, C. Q. Mao and J. Wang, *J. Am. Chem. Soc.*, 2011, *133*, 17560–17563.